



Available online at www.sciencedirect.com

SCIENCE @ DIRECT®

C. R. Chimie 8 (2005) 1336–1350



<http://france.elsevier.com/direct/CRAS2C/>

Full paper / Mémoire

Theoretical aspects of the bonding in acetylide-bridged organometallic dinuclear complexes

Nadia Ouddaï^{a,b,c}, Karine Costuas^b, Mustafa Bencharif^c, Jean-Yves Saillard^b,
Jean-François Halet^{b,*}

^a *Laboratoire de chimie et chimie de l'environnement, université de Batna, Batna, Algeria*

^b *Laboratoire de chimie du solide et inorganique moléculaire, UMR CNRS 6511, Institut de chimie de Rennes, université de Rennes-1, 35042 Rennes cedex, France*

^c *Laboratoire de chimie des matériaux, université de Constantine, Constantine, Algeria*

Received 12 October 2004; accepted after revision 9 December 2004

Available online 07 April 2005

Abstract

The electronic and geometrical structures of a variety of acetylide-bridged organometallic dinuclear complexes ($(ML_n)_2(\mu-C_2)$) ($M = Sc, Ti, W, Ru, Pt$) are analysed and compared by use of extended Hückel and density functional-theory calculations. It is established that all the studied complexes feature the ethyne valence structure, except the titanium species for which resonance forms of ethyne-type and cumulenic-type must be invoked to rationalise its structure. Results indicate that the σ -bonded framework is similar in all complexes and mainly governs the metal–carbon bonding in these species. In all cases but the titanium compound, the σ -type $M-C$ is hardly complemented by π -back-donation from the metals into acceptor C_2 orbitals. The peculiar energy and composition of the HOMOs, which are in general metal–carbon antibonding and carbon–carbon bonding for the metals at the right of the periodic table, can allow the observation of cumulenic structures upon oxidation. **To cite this article:** N. Ouddaï et al., *C. R. Chimie 8 (2005)*.

© 2005 Académie des sciences. Published by Elsevier SAS. All rights reserved.

Résumé

Les structures géométriques et théoriques de divers complexes organométalliques à pont acétylure de formule $(ML_n)_2(\mu-C_2)$ ($M = Sc, Ti, W, Ru, Pt$) sont analysées et comparées à l'aide de calculs en méthodes de Hückel étendue et de la fonctionnelle de la densité. Il est montré que tous les composés étudiés peuvent être décrits à l'aide d'une formule de Lewis de type acétylénique, à l'exception d'une espèce au titane, pour laquelle les deux formes résonantes acétylénique et cumulénique sont nécessaires pour rationaliser sa structure. Les calculs montrent que le mode de liaison σ est similaire dans tous les composés et gouverne majoritairement la liaison métal–carbone. Dans tous les cas, excepté le composé au titane, le retour π des atomes métalliques vers les orbitales acceptrices du ligand C_2 est quasiment absent. L'énergie et la composition des orbitales moléculaires les plus hautes occupées, qui sont antiliantes métal–carbone et liantes carbone–carbone pour les composés de la droite du tableau périodique, laissent entrevoir la possibilité d'espèces cumuléniques après oxydation. **Pour citer cet article :** N. Ouddaï et al., *C. R. Chimie 8 (2005)*.

© 2005 Académie des sciences. Published by Elsevier SAS. All rights reserved.

* Corresponding author.

E-mail address: halet@univ-rennes1.fr (J.-F. Halet).

Keywords: Acetylide complexes; Organometallic complexes; EHT calculations; DFT calculations; Bonding

Mots clés : Complexes acétylures ; Complexes organométalliques ; Calculs EHT ; Calculs DFT ; Liaison

1. Introduction

C_2 is a peculiar simple diatomic molecule [1]. Taken alone, it is not very stable although it can be generated in a carbon arc, is found in comets, or is responsible for the blue light we see in flames. It looks like a dumbbell in which the two carbon atoms are separated from 1.24 Å in the ground state. Such a molecule can easily be stabilised by other atoms or group of atoms. In the realm of organic chemistry, it is contained in ethane, ethene, and acetylene, molecules which are the archetypical references for carbon–carbon single (1.54 Å), double (1.34 Å), and triple (1.20 Å) bonds, respectively. C_2 units are also found in solid state chemistry [2], with different C–C separations depending on its formal electron count, leading to their interpretation as deprotonated ethyne, ethane or acetylene. For instance, a triple bond (1.19 Å) is assumed in CaC_2 ($Ca^{2+}C_2^{2-}$). In $Gd_2Cl_2C_2$ [$(Gd^{3+})_2(Cl^-)_2(C_2^{4-})_2$] [3], the C–C distance in the C_2 units which reside in octahedral cavities is 1.36 Å, corresponding to a double bond. A C–C single bond (1.47 Å) is observed in $Gd_{10}Cl_{18}C_4$ clusters, compatible with the presence of C_2^{6-} fragments within octahedral metallic cages [$(Gd^{3+})_{10}(Cl^-)_{18}(C_2^{6-})_2$] [2b,4]. C_2 can also be observed in numerous molecular organometallic compounds [5]. C_2 can span two mononuclear metal fragments as in $[ScCp^*_2]_2(\mu-C_2)$ ($Cp^* = C_5Me_5$) [6]. Five metallic atoms are caught in huddling around an exposed C_2 fragment in the cluster $Ru_5(CO)_{11}(\mu-PPh_2)_2(\mu-SMe)_2(\mu_5-\eta^4:\eta^5-C_2)$ [7]. C_2 can also be fully encapsulated in a metallic cage as in $[Co_6Ni_2(CO)_{16}(\mu_8-\eta^6:\eta^6-C_2)]^{2-}$ [8].

As in organic or solid state chemistry, the C–C bond length largely varies in these organometallic systems, and different electronic structures can be assigned on the basis of the C–C distance, which can be related to those in acetylene, ethene or ethane or as well. A carbon–carbon separation corresponding to a triple bond is observed in $[ScCp^*_2]_2(\mu-C_2)$ [6] (1.22 Å) or $[Ru(CO)_2Cp]_2(\mu-C_2)$ [9] (1.19 Å) complexes, whereas the C–C bond length of 1.37 Å measured in the binuclear species $[Ta(t-Bu_3SiO)_3]_2(\mu-C_2)$ [10] is more consistent with a C–C double bond. A C–C distance of

1.38 Å observed in $[W(t-Bu_3O)_3]_2(\mu-C_2)$ is rather assigned to a single bond [11]. C–C bond distances are generally more spread out when the number of metal atoms around the C_2 unit increases as in $Ru_5(CO)_{11}(\mu-PPh_2)_2(\mu-SMe)_2(\mu_5-C_2)$ ($d_{C-C} = 1.305$ Å) or $[Co_6Ni_2(CO)_{16}(\mu_8-C_2)]^{2-}$ ($d_{C-C} = 1.48$ Å) previously mentioned. The analogy between this type of compounds and purely organic or inorganic compounds is then less straightforward. Nevertheless, theoretical studies carried out on these high-nuclearity species by Halet and coworkers have shown that the bonding of C_2 with its metallic host follows the Dewar–Chatt–Ducanson model, resulting from an important forward electronic donation from occupied orbitals of the C_2 fragment toward acceptor metallic molecular orbitals (MO), but also from a back-donation from metallic orbitals into vacant C_2 orbitals [12]. Such a bonding mode is in turn comparable to that previously established for acetylenic complexes [13] and absorbed acetylene on metallic surfaces [14].

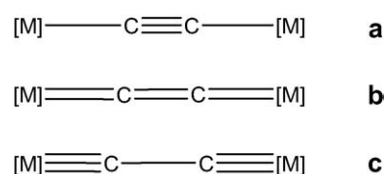
Following these previous studies carried out on encapsulated and exposed C_2 -containing organometallic compounds [12], we have recently investigated the bonding and electronic structure of dinuclear $(ML_n)_2(\mu-C_2)$ complexes in which the C_2 entity is both end-capped by a metallic fragment. These compounds are of interest being thought as models for molecular-scale wires [5]. We report in this paper the main results obtained via extended Hückel theory (EHT) and density functional-theory (DFT) calculations on homometallic compounds containing metal fragments with π -acceptor ligands such as $[Ru(CO)_2Cp]_2(\mu-C_2)$ [9] which have been little studied [15,16]. Dinuclear compounds with π -donor ligands such as $[W(t-Bu_3O)_3]_2(\mu-C_2)$ have not been considered, having been extensively studied previously [10b,11b,17].

2. Structural considerations and electron counts

Several homo- and hetero-dinuclear $(ML_n)_2(\mu-C_2)$ complexes have been structurally characterised. They are reported in Table 1. In all those with π -acceptor

ligands (top of Table 1), a nearly linear M–C–M backbone is found and a short carbon–carbon distance, ca. 1.20–1.25 Å, is measured. On the basis of such a C–C separation, the electronic structure of these compounds seems consistent with valence bond structure **A** rather than valence bond structures **B** or **C** (see Scheme 1) which feature compounds with π -donor ligands.

(ML_n)₂(μ -C₂) complexes under investigation, i.e. those with π -acceptor ligands, can be divided in few groups depending on the nature of the metal, its electronic configuration and the number of surrounding ancillary ligands L. A partition according to the metal *d* configuration gives five groups. Note that this con-



Scheme 1.

figuration is obtained assuming C₂²⁻ ethynediide dianion. One group is made by early-transition metals (scandium and titanium triads) with a d⁰ or d¹ configuration. Molecules in this group consist of Cp₂M or Cp₂ML fragments bonded to the C₂ bridge. Interestingly, they do not conform to the 18-electron rule. Formal counts of 14 and 16 electrons are achieved for the scandium

Table 1

X-ray characterised acetylide-bridged organometallic binuclear complexes (ML_n)₂(μ -C₂)

Compound, structure type ^a	Metal <i>d</i> configuration	<i>d</i> _{C–C} (Å)	References
<i>Homo-dinuclear compounds with π-acceptor ligands</i>			
[ScCp* ₂] ₂ (μ -C ₂), A	d ⁰	1.224(9)	[6]
[SmCp* ₂ (THF)] ₂ (μ -C ₂), A	d ⁰	1.213(10)	[18]
[TiCp ₂ (PMe ₃) ₂] ₂ (μ -C ₂), A/B ^a	d ¹	1.253(2)	[19]
[ZrCp ₂ C(SiMe ₃)CH(SiMe ₃) ₂] ₂ (μ -C ₂), A	d ⁰	1.212(12)	[20]
[ZrCp ₂ NH(<i>t</i> -Bu)] ₂ (μ -C ₂), A	d ⁰	1.226(7)	[21]
[HfCp* ₂ (CCH)] ₂ (μ -C ₂), A	d ⁰	1.24(3)	[22]
[W(CO) ₃ Cp] ₂ (μ -C ₂), A	d ⁴	1.18(3)	[23]
[W(CO) ₃ (η ⁵ -C ₅ H ₄ Me)] ₂ (μ -C ₂), A	d ⁴	1.216(9)	[24]
[Mn(CO) ₅] ₂ (μ -C ₂), A	d ⁶	1.201(2)	[25]
[Re(CO) ₅] ₂ (μ -C ₂), A	d ⁶	1.195(33)	[26]
[Fe(CO) ₂ Cp*] ₂ (μ -C ₂), A	d ⁶	1.206(6)/1.211(6)	[27]
[Ru(CO) ₂ Cp] ₂ (μ -C ₂), A	d ⁶	1.19(1)	[9]
[Ru(PPh ₃) ₂ Cp] ₂ (μ -C ₂), A	d ⁶	1.230(7)	[28]
[Pt(PMe ₃) ₂ I] ₂ (μ -C ₂), A	d ⁸	1.179(48)	[29]
[Pt(PPh ₃) ₂ Cl] ₂ (μ -C ₂), A	d ⁸	1.221(9)	[30]
[(OC)(C ₆ F ₅) ₂ Pt][{C(Me)OEt}(PEt ₃) ₂ Pt] ₂ (μ -C ₂), A	d ⁸	1.22(3)	[31]
{[Pt(<i>t</i> -Bu-tpy)] ₂ (μ -C ₂)} ²⁺ , A	d ⁸	1.118(11)	[32]
[Au(PMe ₃) ₂] ₂ (μ -C ₂), A	d ¹⁰	1.21(2)	[33]
[Au(PEt ₃) ₂] ₂ (μ -C ₂), A	d ¹⁰	1.21(2)	[33]
[Au(PPhMe ₂) ₂] ₂ (μ -C ₂), A	d ¹⁰	1.216(7)	[33]
[Au(P(C ₆ H ₅ -3)] ₂ (μ -C ₂), A	d ¹⁰	1.19(2)	[34]
[Au(P(C ₆ H ₄ Me-3)] ₂ (μ -C ₂), A	d ¹⁰	1.19(2)	[34]
[Au(PCy ₃) ₂] ₂ (μ -C ₂), A	d ¹⁰	1.19(1)	[35]
[AuPPh(naphthyl)] ₂ (μ -C ₂), A	d ¹⁰	1.225(34)	[36,37]
[AuPPh ₂ (naphthyl)] ₂ (μ -C ₂), A	d ¹⁰	1.222(16)	[36,37]
[AuPPhFc ₂] ₂ (μ -C ₂), A	d ¹⁰	1.196(12)	[37]
<i>Homo-dinuclear compounds with π-donor ligands</i>			
[Ta(<i>t</i> -Bu ₃ SiO) ₃] ₂ (μ -C ₂), B	d ⁰	1.37(4)	[10]
[W(<i>t</i> -BuO) ₃] ₂ (μ -C ₂), C	d ⁰	1.38(2)/1.34(3)	[11]
<i>Hetero-dinuclear compounds</i>			
[RuCp(PMe ₃)] ₂ [ZrClCp ₂] ₂ (μ -C ₂), A	d ⁰ /d ⁶	1.251(20)	[38]
[ReCp*(NO) ₃ PPh ₃][Pd(PEt ₃) ₂ Cl] ₂ (μ -C ₂), A	d ⁶ /d ⁸	1.21(1)	[39]

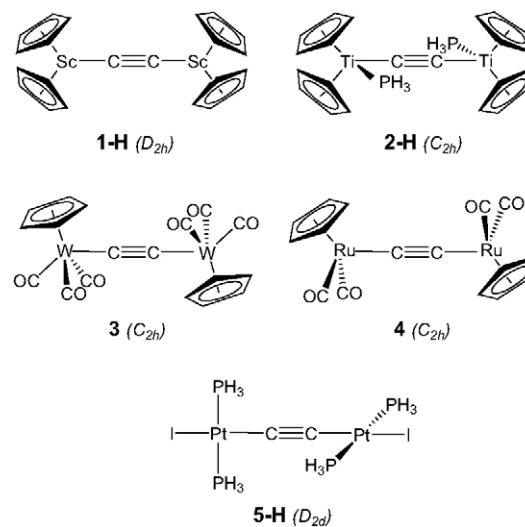
^a See text.

and samarium compounds, respectively. For the titanium triad compounds, a count of 16 electrons is also obtained for the Ti heavy congeners, Zr and Hf, whereas for titanium itself, a formal count of 17 electrons is reached assuming C_2^{2-} . Compounds with mid-transition metal (chromium triad) contain $d^4 ML_6$ fragments framing the C_2 dumb-bell. They conform to the 18-electron rule. This is also the case for compounds made by mid-to-late transition metals (manganese and iron triads), which are built from pseudo-octahedral $d^6 ML_5$ fragments. A 16-electron configuration for each metal is achieved for species containing T-shaped late transition metal (platinum) $d^8 ML_3$ fragments linked to C_2 . Finally, the last group is constituted of molecules with very-late transition metal (gold) $d^{10} M-L'$ fragments. In the latter species, each metal in linear $L-M-L'$ conformation bears 14 electrons.

EHT and DFT calculations were carried out on complexes belonging to different groups (see the Appendix) in order to provide particular insight regarding various marked differences (if any) between this series of complexes. In order to reduce the computational effort, calculations were conducted on complex models $[ScCp_2]_2(\mu-C_2)$ (**1-H**), $[TiCp_2(PH_3)]_2(\mu-C_2)$ (**2-H**), and $[Pt(PH_3)_2I]_2(\mu-C_2)$ (**5-H**) used to mimic $[ScCp_{*2}]_2(\mu-C_2)$ [6] (**1**), $[TiCp_2(PMe_3)]_2(\mu-C_2)$ [19], (**2**), and $[Pt(PMe_3)_2I]_2(\mu-C_2)$ [29] (**5**), respectively, as well as on complexes $[W(CO)_3Cp]_2(\mu-C_2)$ [23] (**3**) and $[Ru(CO)_2Cp]_2(\mu-C_2)$ [9] (**4**). Calculations were made with symmetry constraints: D_{2h} symmetry for **1-H**, C_{2h} symmetry for **2-H**, **3** and **4**, and D_{2d} symmetry for **5-H** (see Scheme 2).

3. Qualitative MO analysis

Before discussing DFT results concerning the bonding in these complexes, we think that a qualitative analysis based upon EHT offers an instructive general perspective. Indeed, the bonding between the C_2 dumb-bell and metallic termini can qualitatively be understood using the frontier molecular orbitals (FMO) of the C_2^{2-} dianion and two cationic organometallic fragments. Let us remind first that the former fragment is rather versatile throughout the energy and nodal properties of its FMOs and able to act as a formal donor of different numbers of electrons, depending on the electronic demands of the metallic fragments which it interacts



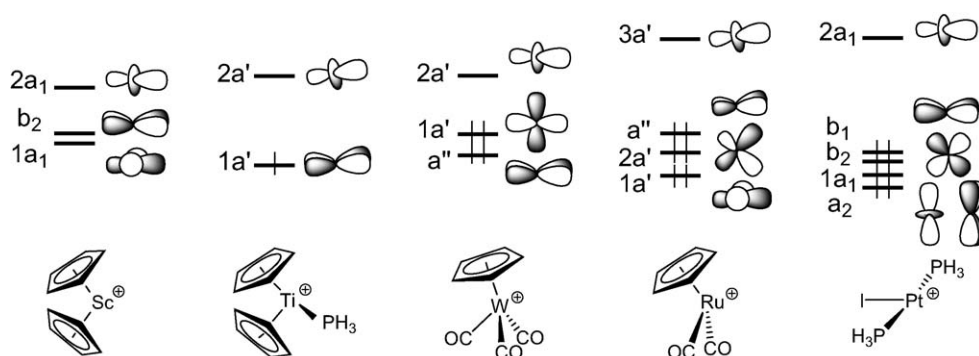
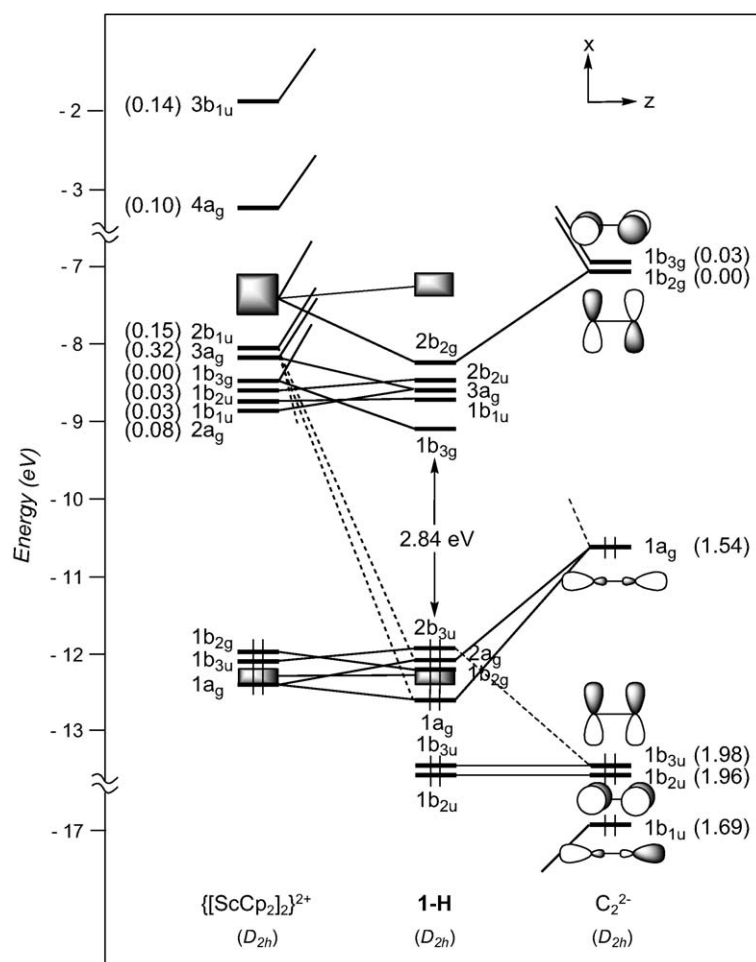
Scheme 2.

with. The orbitals that may be involved in interaction with the metallic end-groups are the σ_s and σ_p non-bonding and π bonding occupied FMOs, and the π^* bonding vacant FMOs [13].

3.1. d^0-d^0 and d^1-d^1 $(ML_n)_2(\mu-C_2)$ complexes

We commence with an analysis of the d^0-d^0 $(ML_n)_2(\mu-C_2)$ complexes. In $ScCp_2]_2(\mu-C_2)$, **1-H**, the C_2 entity is framed by two $ScCp_2$ fragments. The three FMOs of each metal fragment can be derived from the t_{2g} -like set of normal MCp_2 complexes such as ferrocene. Fig. 1 illustrates the nodal properties of these three FMOs (two of σ type, $1a_1$ and $2a_1$, and one of π type, b_2), split apart in energy and somewhat hybridised in the direction of an in-coming ligand, due to the bending of the Cp rings back from the parallel geometry [40]. Consequently, the dinuclear scandium fragment exhibits a set of six FMOs (out-of-phase $1b_{1u}$, $1b_{3g}$, and $2b_{1u}$, and in-phase $2a_g$, $1b_{2u}$, and $3a_g$ combinations under D_{2h} symmetry (see the left hand-side of Fig. 2), some of which might play a prime role in coordinating the C_2 unit.

The bonding between the metallic and the carbon fragments is essentially governed by strong σ -type interactions involving the low-lying C_2 orbitals $1b_{1u}$ and $1a_g$ with the metallic FMOs $3a_g$ and $4a_g$, and $2b_{1u}$ and $3b_{1u}$, respectively. Digits given in brackets in Fig. 2 which indicate the electron occupation of FMOs after interaction between the component fragments, illustrate

Fig. 1. EHT FMOs of different ML_n fragments.Fig. 2. EHT orbital diagram for the model complex $[ScCp_2]_2(\mu-C_2)$ (**1-H**). FMO occupations after interaction are given in brackets.

numerically the degree of electron donation from the C_2^{2-} spacer toward the metallic fragment. With metals formally d^0 , the σ -type Sc–C bonding cannot be complemented by π -type back-donation from the metallic fragment into the acceptor C_2 π^* orbitals. Some π -type Sc–C bonding could be expected resulting from stabilising interactions between the low-lying occupied π orbitals of C_2 and the high-lying vacant metallic FMOs. It turns out that the large energy difference between them prevents significant interactions to occur. This is reflected in the electron occupation of the π orbitals of C_2 close to two after interaction (see Fig. 2). It can then be considered that only σ -type Sc–C bonding is present in complex **1-H**. This situation is reminiscent of ethyne.

The geometry of the d^1 – d^1 complex $[TiCp_2(PMe_3)]_2(\mu-C_2)$, **2**, can formally be derived from that of compound **1**, by adding a σ bonding ligand on metal centres *cis* to the C_2 entity. A fragment analysis of **2-H**,

used to mimic compound **2**, with the ethyniide anion on one hand and the metal fragment $\{[TiCp_2(PH_3)]_2\}^{2+}$ on the other, leads us to first consider the bonding properties of the unsymmetrical $[TiCp_2(PH_3)]^+$ fragment. Isolobal to $[CH_2]^+$, it has two FMOs, $1a'$ and $2a'$ under C_s symmetry which extend in the yz plane between the Cp rings (see Fig. 1) [40]. They intermix a little being of the same symmetry. Bringing two non-interacting $[TiCp_2(PH_3)]^+$ fragments together gives rise to a set of four FMOs which span $2b_u$, $3a_g$, $1b_u$, and $2a_g$ under C_{2h} symmetry (Fig. 3). Only the $2a_g$ FMO is occupied for the metal d^1 configuration. Important σ donation occurs through strong interactions between the C_2 σ -donor orbitals ($1a_g$ and $2a_g$) with metallic orbitals of the same symmetry. Conversely to compound **1**, the σ -bonded framework is complemented by Ti–C π bonding due to attractive interactions between one component, $1b_u$, of the occupied π C_2 orbitals and acceptor metallic FMOs, $2b_u$ and $1b_u$, on one hand, and between

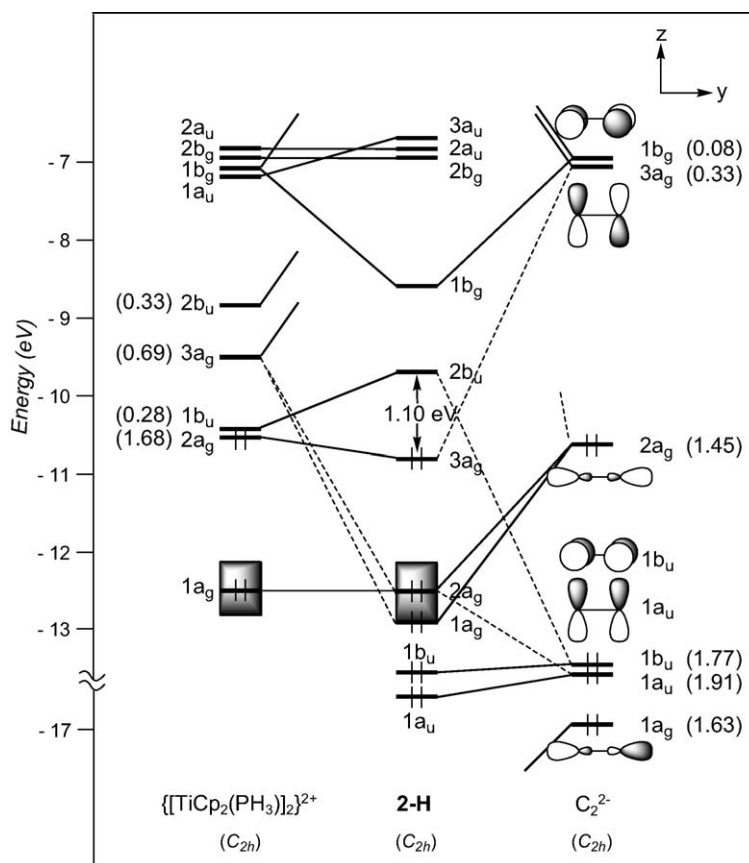
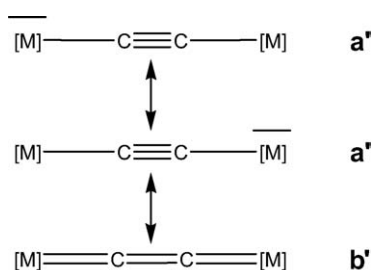


Fig. 3. EHT orbital diagram for the model complex $[TiCp_2(PH_3)]_2(\mu-C_2)$ (**2-H**). FMO occupations after interaction are given in brackets.

one component, $3a_g$, of the $\pi^* C_2$ orbitals and the metallic $2a_g$ FMO on the other hand. The out-of-phase combination of the former and the in-phase of the latter are the LUMO and HOMO, respectively, of compound **2-H**. These rather strong interactions are reflected in the electron occupations after interaction of the involved FMOs (see Fig. 3). Partial depopulation of one π component and partial population of one π^* component of C_2 after interaction with the metallic fragment contribute to weaken the C–C bond and to strengthen the Ti–C bonds. This is consistent with dominant cumulenic valence structure **B'** with three bonding π doublets (Scheme 3), often proposed in the literature to describe the electronic structure of **2** [19]. Nevertheless, population of the $\pi^* C_2$ orbital involved in Ti–C bonding being far from complete, participation of the limiting valence structure pattern **A'** with two bonding and one non-bonding π doublets (Scheme 3) cannot be excluded.

3.2. $d^4-d^4 (ML_n)_2(\mu-C_2)$ complexes

Only two $d^4-d^4 (ML_n)_2(\mu-C_2)$ complexes have been characterised with metal fragments containing acceptor ligands, $[W(CO)_3Cp]_2(\mu-C_2)$, **3** [23], and his derivative $[W(CO)_3(\eta^5-C_5H_4Me)]_2(\mu-C_2)$ [24]. In these complexes, the metal centres adopt a 'four-legged piano-stool' geometry [41], a high seven-coordination which allows them to achieve the 18-electron configuration. A fragment analysis of **3** can be done considering the molecule made of a C_2 entity spanning two distorted octahedral $d^4 ML_6$ end-groups. The frontier orbitals of such a scarce metal fragment can be derived from those of a pseudo-octahedral $MCpL_3$ arrangement upon tilting of the Cp ring [41]. They are illustrated in Fig. 1. They consist of three low-lying FMOs, a'' (π -type), $1a'$ and $2a'$ (σ -type), which descend from the ' t_{2g} ' set. In- and out-of-phase combinations of the FMOs of two non-interacting $[W(CO)_3Cp]^+$ fragments give rise to six



Scheme 3.

FMOs which span $2b_u$ (σ -type), $2a_g$ (σ -type), $1a_g$ (δ -type), $1b_u$ (π -type), $1b_g$ (δ -type), and $1a_u$ (π -type), under C_{2h} symmetry. The two higher are vacant for d^4 configuration (see Fig. 4).

A detective analysis of the interaction diagram of **3** shown in Fig. 4, reveals that the dominant interactions are again of σ -type, involving the acceptor metallic $2b_u$ and $2a_g$ FMOs and the σ -donor orbitals $1b_u$ and $1a_g$ of the dicarbon moiety. Small electron occupations following interaction of the π -acceptor C_2 orbitals with the metal fragment, 0.10 and 0.15, indicate that the W–C σ -bonding is hardly complemented by back-donation from the occupied metallic FMOs toward C_2 . The HOMOs result from four-electron repulsive interactions between metal FMOs, $1a_u$ and $1b_u$, and π -type C_2 orbitals and are consequently W–C antibonding and C–C bonding.

3.3. $d^6-d^6 (ML_n)_2(\mu-C_2)$ complexes

In the $d^6-d^6 (ML_n)_2(\mu-C_2)$ complex series, the C_2 unit spans ML_5 fragments with different metals and surrounding ligands (see Table 1). The bonding in $[M(CO)_5]_2(\mu-C_2)$ ($M = Mn, Re$) has been studied previously with the aid of DFT calculations and therefore will not be discussed [16,26]. We rather devote our attention here to $[Ru(CO)_2Cp]_2(\mu-C_2)$ [9], **4**, the diphosphine relative of which, namely $[Ru(PPh_3)_2Cp]_2(\mu-C_2)$, undergoes facile reversible oxidations [28]. Each $Ru(CO)_2Cp$ fragment presents a ' t_{2g} ' set of d-type orbitals ($2a'$ and a'' of π -type, $1a'$ of σ -type) situated below a radial hybrid orbital ($3a'$) (see Fig. 1) [42]. Out-of-phase and in-phase combinations of the orbitals of two non-interacting metal fragments give rise to a set of eight FMOs, four of σ -type, $1a_g$ and $1b_u$ (descending from $1a'$) and $3a_g$ and $3b_u$ (descending from $3a'$), and four of π -type, $1b_g$ and $1a_u$ (descending from a'') and $2a_g$ and $2b_u$ (descending from $2a'$) (see Fig. 5).

Here again, strong σ -type interactions which occur between the $3b_u$ and $3a_g$ metallic FMOs and the σ -donor C_2 orbitals, are mainly responsible for the M–C bonding in **4** (see electron occupation numbers after interaction in Fig. 5). This bonding is complemented by a rather weak π -type back-donation from occupied metallic FMOs into the π^* acceptor orbitals of C_2 $1b_g$ and $2a_g$. Indeed, the predominant Ru–C π -type interactions are actually filled–filled interactions involving occupied metal π MOs and occupied π MOs of C_2 , $2b_u$ and

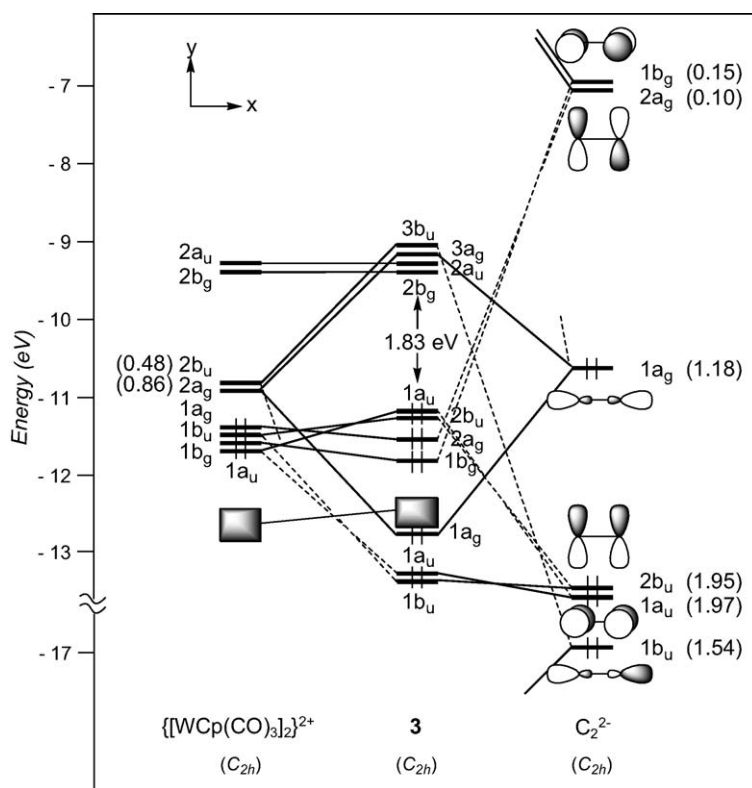


Fig. 4. EHT orbital diagram for the complex $[\text{W}(\text{CO})_3\text{Cp}]_2(\mu\text{-C}_2)$ (**3**). FMO occupations after interaction are given in brackets.

$1a_u$. Interestingly, the out-of-phase combination becomes the HOMO of the system, highly delocalised over the entire $\text{M}-\text{C}_2-\text{M}$ backbone. As expected, analogous results are observed for the compound $[\text{Fe}(\text{CO})_2\text{Cp}^*]_2(\mu\text{-C}_2)$ which contains similar ML_5 end-groups.

3.4. d^8-d^8 (ML_n) $_2(\mu\text{-C}_2)$ complexes

Few ethynediyl platinum complexes have been reported. There is a current interest for these compounds, some of which have recently been shown to display luminescence behaviour [32]. They all contain d^8 ML_3 T-shaped fragments (see Table 1). The model $[\text{Pt}(\text{PH}_3)_2\text{I}]_2(\mu\text{-C}_2)$, **5-H**, of D_{2d} symmetry, was taken as a representative of this series¹. The FMOs of a d^8 $[\text{Pt}(\text{PH}_3)_2\text{I}]^+$ fragment [43], drawn in Fig. 1, consist of

one hybrid σ -type FMO, $2a_1$, above a set of four d orbitals, two of π -type (b_1 and b_2), one of σ -type ($1a_1$), and one of δ -type (a_2). The FMOs of the $[\text{I}(\text{PH}_3)_2\text{Pt}^+\text{Pt}(\text{PH}_3)_2\text{I}]^{2+}$ fragment of D_{2d} symmetry are essentially the in- and out-of-phase combinations of the orbitals shown in Fig. 6: two vacant high-lying σ -type orbitals, $2a_1$ and $2b_2$, and a set of eight occupied low-lying d -type orbitals. The former interact strongly with the σ -type donor C_2 orbitals, $1b_2$ and $1a_1$. As in the case of **4**, back-donation from the occupied metallic FMOs into the vacant π^* C_2 orbitals is rather weak. Therefore, σ -type interactions mainly account for the Pt–C bonding in these species. Interestingly, some participation of the π C_2 orbitals is noted in the HOMO, $5e$, of the complex, which mainly derived from the π -type $3e$ metallic FMO.

¹ Experimentally, the coordination planes around the Pt atoms can be almost coplanar as in $[(\text{OC})(\text{C}_6\text{F}_5)_2\text{Pt}][\{\text{C}(\text{Me})\text{OEt}\}(\text{PEt}_3)_2\text{Pt}]\mu\text{-C}_2$ (dihedral angle of 6.7°) [31], nearly staggered as in $[\text{Pt}(\text{PMe}_3)_2\text{I}]_2(\mu\text{-C}_2)$ (dihedral angle of 89.8°) [29] or

$[\text{Pt}(\text{PPh}_3)_2\text{Cl}]_2(\mu\text{-C}_2)$ (dihedral angle of 82°) [30], or somewhat twisted as in $[\text{Pt}(t\text{Bu-tpy})]_2(\mu\text{-C}_2)^{2+}$ (dihedral angle of 35.83°) [32]. A twist of the metal moieties with respect to each other for some of them may help to relieve the steric strain arising from the bulky surrounding ligands.

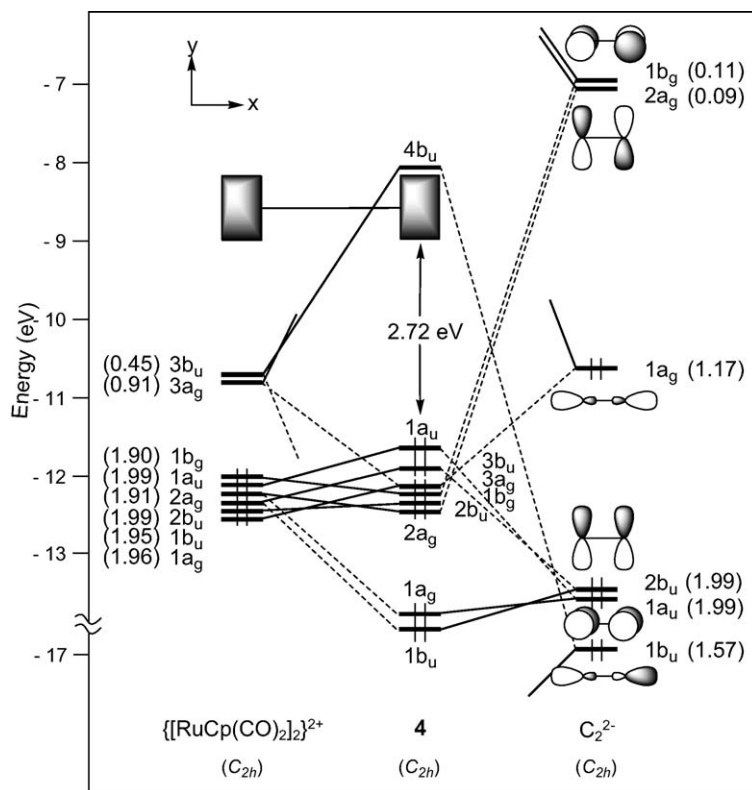


Fig. 5. EHT orbital diagram for the complex $[\text{Ru}(\text{CO})_2\text{Cp}]_2(\mu\text{-C}_2)$ (**4**). FMO occupations after interaction are given in brackets.

3.5. $d^{10}\text{-}d^{10}$ (ML_n) $_2(\mu\text{-C}_2)$ complexes

The last series is made of the $d^{10}\text{-}d^{10}$ gold complexes $(\text{AuPR}_3)_2(\mu\text{-C}_2)$. With AuPR_3 isolobal to H [44], the bonding in these complexes, not discussed here, is really comparable to that encountered in ethyne, with strong σ -type Au–C bonding.

4. Carbon–carbon bond strength

From Table 2 it is apparent that the EHT computed C–C overlap populations are quite similar in all studied complexes, ca. 1.90, except for the titanium compound **2-H** where the C–C overlap population is markedly smaller (1.78). Surprisingly, the net charges of the C_2 dumb-bell somewhat differ with carbon atoms more negatively charged in early-transition metal complexes (see Table 2). Indeed, the electron loss from the C_2^{2-} donor orbitals is more important in compounds **3**, **4**, and **5-H** than in compound **1-H**. This should lead to a weaker C–C bond in the former.

It is noteworthy that, despite similar net charges on the C_2 entity, -1.18 vs. -1.14 , the M–C and C–C bonding differ in the scandium and the titanium complexes. In the former, Sc–C bonding results only from some electron donation from C_2^{2-} to the metal fragments, whereas Ti–C bonding is due to more important donation from C_2^{2-} toward the titanium fragments and some back-donation from the metals into vacant C_2^{2-} orbitals. Although both donation and back-donation compensate each other in the titanium complex to lead to C_2 charge comparable to that of **1-H**, they both contribute to a weakening of the carbon–carbon bond with respect to that in the scandium species.

5. DFT analysis

DFT calculations were performed on model compounds **1-H**, **2-H**, **3**, **4**, and **5-H** in order to give support to the qualitative analysis and to bring additional results on their electronic properties.

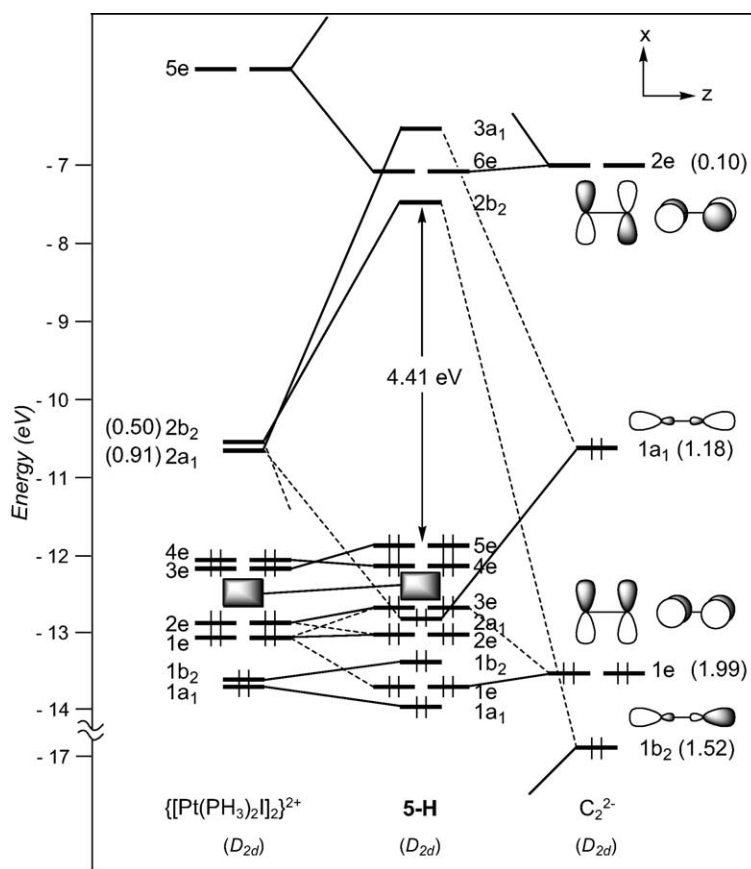


Fig. 6. EHT orbital diagram for the model complex and $[\text{Pt}(\text{PMe}_3)_2\text{I}]_2(\mu\text{-C}_2)$ (**5-H**). FMO occupations after interaction are given in brackets.

Table 2
EHT computed characteristics for different models complexes $(\text{ML}_n)_2(\mu\text{-C}_2)$

Complex	1-H	2-H	3	4	5-H
Metal <i>d</i> configuration	d^0	d^1	d^4	d^6	d^8
	<i>C₂ FMO occupations</i>				
σ_u/σ_g	1.54/1.69	1.45/1.63	1.18/1.54	1.17/1.57	1.18/1.52
π^*	0.00/0.03	0.08/0.33	0.10/0.15	0.11/0.09	0.10/0.10
	<i>Overlap population</i>				
C–C	1.95	1.78	1.88	1.89	1.89
	<i>Atomic net charge</i>				
C	–0.59	–0.57	–0.43	–0.46	–0.43

5.1. Molecular geometries

The pertinent distances of the DFT optimised geometries for the different studied complexes are collected in Table 3 with few experimental estimates for comparison. The agreement is good overall. The computed carbon–carbon bond length in the ethynyl spacer is slightly overestimated by 2–5%. This is fully accept-

able considering that the corresponding experimental values were measured with rather large uncertainties. Interestingly, except for the titanium compound where it is slightly longer, the C–C separation is nearly constant, ca. 1.24 Å, regardless of the metal bonded. This gives support to the comparable C–C overlap populations computed for complexes **1-H**, **3**, **4**, and **5-H** (see above). The calculated M–C bond lengths are underes-

Table 3
Selected DFT optimised distances (Å) for different models complexes $(ML_n)_2(\mu-C_2)^a$

Complex	1-H	2-H	3	4	5-H
C–C	1.254 <i>1.224(9)</i>	1.276 <i>1.253(2)</i>	1.240 <i>1.18(3)</i>	1.235 <i>1.19(1)</i>	1.238 <i>1.179(48)</i>
M–C ^b	2.186 <i>2.194(7)</i>	2.018 <i>2.051(2)</i>	2.141 <i>2.172(22)</i> <i>2.148(20)</i>	2.053 <i>2.04(1)</i> <i>2.05(1)</i>	1.968 <i>1.973(30)</i> <i>1.980(38)</i>
M–Cp ^b	2.192 <i>2.171</i>	2.113 <i>2.080(2)</i> <i>2.079(2)</i>	2.046	2.049	
M–P		2.599 <i>2.549(1)</i>			2.293 <i>2.302(11)</i> ^c
M–C(O)			1.995	1.848 <i>1.87(1)</i> ^c	
Pt–I					2.721 <i>2.649(3)</i> ^c

^a Corresponding experimental distances are given in italics when available.

^b Cp centroid.

^c Average distance.

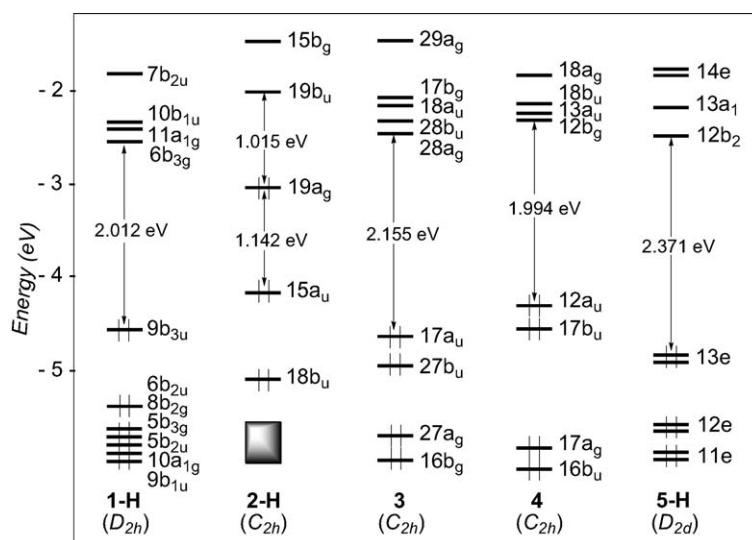


Fig. 7. DFT diagrams for the model complexes **1-H**, **2-H**, **3**, **4**, and **5-H**.

timated by only 2–3% and fall in the range of M–C single bond distances generally measured experimentally for this kind of complex.

5.2. MOs

The DFT MO diagrams of the studied models complexes are shown in Fig. 7. They are qualitatively similar to the EHMO diagrams given earlier. Except for the titanium compound **2-H**, large HOMO–LUMO gaps, ca. 2 eV, are computed, regardless of the electron count around the metal atoms, 14 for Sc in **1-H**, 18 for W in **3**, 18 for Ru in **4**, and 16 for Pt in **5-H**. Some ethynediyl complexes undergo one-electron oxidation processes [28]. Therefore, it is informative to look at the energy and composition of the HOMOs to better discuss of the structural changes which may occur upon oxidation.

To this end, a Mulliken atomic orbital population analysis and plots of the HOMO and HOMO-1 are given in Table 4 and Fig. 8, respectively. In **1-H**, the HOMO and HOMO-1 lie at rather low energy and are largely separated. They are heavily weighed on C₂ (64% and 84%). They derive from the C₂ π orbitals, somewhat mixed with Sc–Cp orbitals.

DFT MO diagrams of the tungsten and ruthenium complexes, **3** and **4**, are quite similar with comparable HOMO–LUMO gaps, ca. 2eV, and nearly degenerated HOMO and HOMO-1 lying at relatively high energy. Examination of their composition confirms their delocalisation over the entire M–C₂–M chain and features an appreciable component from the C₂ unit (47% and 34% in **3**, 62 and 71% in **4** for the HOMO and HOMO-1, respectively). The contour plots of these orbitals, illustrated in Fig. 8, confirm the EHT results,

Table 4

Energies (ϵ , eV) and percentage compositions of selected orbitals (MO) in the HOMO–LUMO region of different models complexes $(ML_n)_2(\mu-C_2)$

1-H						
MO	11a _{1g}	6b _{3g}	9b _{3u}	6b _{2u}	8b _{2g}	5b _{3g}
ϵ	-2.368	-2.548	-4.560	-5.394	-5.724	-5.826
occ	0	0	2	2	2	2
Sc	87	70	0	11	14	8
C ₂	0	10	64	84	0	0
C(Cp)	12	17	35	1	79	87
2-H						
MO	15b _g	19b _u	19a _g	15a _u	18b _u	14b _g
ϵ	-1.465	-2.007	-3.022	-4.165	-5.066	-5.584
occ	0	0	2	2	2	2
Ti	56	61	67	0	13	19
C ₂	7	15	9	58	67	1
P	0	0	5	0	2	0
C(Cp)	24	13	10	41	6	69
3						
MO	28b _u	28a _g	17a _u	27b _u	27a _g	16b _g
ϵ	-2.271	-2.409	-4.565	-4.866	-5.645	-5.896
occ	0	0	2	2	2	2
W	22	15	27	31	55	54
C ₂	14	16	47	34	2	3
C(Cp)	14	12	4	7	0	3
CO	50	56	15	24	37	35
4						
MO	13a _u	12b _g	12a _u	17b _u	17a _g	16b _u
ϵ	-2.212	-2.268	-4.262	-4.519	-5.804	-6.046
occ	0	0	2	2	2	2
Ru	39	42	23	21	31	31
C ₂	1	0	62	71	8	11
C(Cp)	20	22	9	1	39	33
CO	37	34	2	3	16	16
5-H						
MO	13a ₁	12b ₂	13e	12e	11e	12a ₁
ϵ	-2.179	-2.486	-4.857	-5.582	-5.874	-6.164
occ	0	0	4	4	4	2
Pt	32	30	30	6	4	88
C ₂	9	13	43	0	26	4
I	11	17	26	89	66	2
P	26	30	0	0	1	3

i.e. these MOs are π -type in character, antibonding between the metal centres and the C₂ linkage and bonding between the carbon atoms. No electrochemical study has been carried out on compounds **3** and **4**. On the other hand, studies performed on the parent molecule of **4**, $[Ru(PPh_3)_2Cp]_2(\mu-C_2)$, which contains more electron-donating groups, indicate that it can undergo several one-electron oxidations [28]. Interestingly,

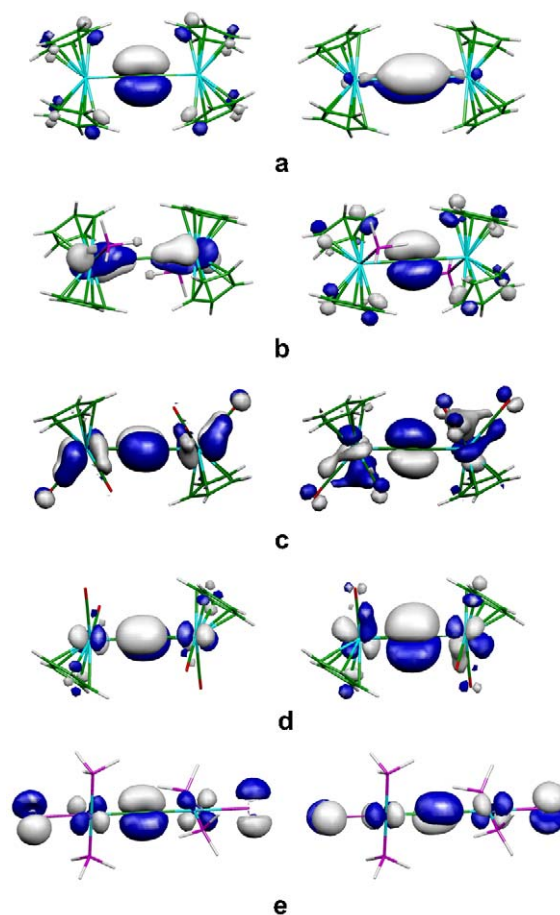


Fig. 8. DFT contour plots of the HOMO (left) and HOMO-1 (right) for the model complexes **1-H** (a), **2-H** (b), **3** (c), **4** (d), and **5-H** (e). Contour values are ± 0.035 (e/bohr^3)^{1/2}.

X-ray measurements on the dicationic species reveal a shortening of the Ru–C bond and some lengthening of the C–C bond [28]. This change in Ru–C and C–C bond lengths upon oxidation can in turn be rationalised by the nodal properties of the two nearly degenerate HOMOs which are partially depopulated. Whereas $[Ru(PPh_3)_2Cp]_2(\mu-C_2)$ features the ethyne valence structure **A**, the dication $\{[Ru(PPh_3)_2Cp]_2(\mu-C_2)\}^{2+}$ is best described by the fully double-bonded cumulenic valence structure **B** (see Scheme 1).

A somewhat larger HOMO–LUMO gap, 2.371 eV, is computed for the platinum model complex **5-H**. This is due to the degenerate HOMOs 3e which lies at lower energy. Analogously to compounds **3** and **4**, they are delocalised over the metal–carbon chain (30% Pt and 30% C₂), and exhibit the same nodal properties (see

Fig. 8). Let us note that the iodine participation in these orbitals is quite important because of a strong π -interaction between the lone pairs of the halogen atoms and the Pt d-type orbitals.

The EHT MO diagram of the titanium complex **2-H**, suggested that its electronic structure differs from that of the others. This is confirmed by DFT calculations: smaller HOMO–LUMO gap, 1.015 eV, and HOMO and HOMO-1 of different energy and nodal properties (see Fig. 8). The HOMO-1, derived from one component of the π C₂ orbitals, is mainly carbon in character (58%) and, to a lesser extent, Cp in character. The HOMO, also of π -type is slightly more delocalised over the M–C₂–M backbone (67% metal, 9% C₂) and is Ti–C bonding and C–C antibonding, resulting from a bonding interaction between metallic orbitals and one component of the π^* C₂ orbitals. This strongly differs from the nodal properties of the HOMO in the other systems which generally are M–C antibonding and C–C bonding (vide supra).

Is **2-H** a dimetalla–cumulene system that must be described with valence structure **B'**? The fact that the HOMO involves one component of the π^* orbitals of the C₂ unit gives support to such a structural pattern. Nevertheless, carbon participation in the MO is rather weak and the resonant ethyne valence structure **A'** cannot be neglected in the description of the electronic structure of **2-H**. Participation of structure patterns **A'** and **B'** in the electronic structure of the titanium species is supported by the optimised C–C bond distance, 1.276 Å (1.253 Å in **2**) which is intermediate between a double and a triple bond. A HOMO rather high in energy and lying in the middle of a large energy gap suggests that oxidation of **2** should be possible. Indeed, preliminary DFT calculations on the dication model complex [**2-H**]²⁺ indicate some increasing of the Ti–C bond (from 2.018 to 2.104 Å) and some shortening of the C–C bond (from 1.276 to 1.256 Å), consistent with valence formula **A**. A significant HOMO–LUMO gap of 0.79 eV is computed. Such results suggest that electrochemical studies on **2** should be encouraged.

It is noteworthy that with the other metals of the Ti triad, Zr and Hf, ethynediyl complexes with two electrons less and shorter C–C bonds have been characterised (see Table 1). With formal d⁰ metal centres, the electronic structure of these zirconium and hafnium species is comparable to that of the scandium complex **1-H**, i.e. best described by structure pattern **A**.

6. Conclusion

In summary, this study has highlighted the electronic structure of diverse acetylide-bridged organometallic binuclear complexes. Using EHT and DFT calculations, we have established that all the studied complexes feature the ethyne valence structure **A** regardless of the metal d configuration, except the titanium species **2** for which resonance forms of ethyne-type (structure **A**) and cumulenic-type (structure **B**) must be invoked to rationalise its structure. Results indicate that the σ -bonded framework is similar in all complexes and mainly governs the metal–carbon bonding in these species. In all cases but the titanium compound **2**, the σ -type M–C is hardly complemented by π -back-donation from the metals into acceptor C₂ orbitals. As noted previously [17], the C₂ π^* orbitals are well removed in energy from the donor metallic orbitals, and back bonding is therefore limited. The peculiar composition of the HOMOs, which are metal–carbon antibonding and carbon–carbon bonding in general for the metals at the right of the periodic table, can allow the observation of cumulenic structures **B** upon oxidation. This is nicely illustrated experimentally for the dicationic {[Ru(PPh₃)₂Cp]₂(μ -C₂)}²⁺ species [28].

Acknowledgements

We thank the ‘Pôle de calcul intensif de l’Ouest’ (PCIO) of the University of Rennes and the ‘Institut de développement et de ressources en informatique scientifique’ (IDRIS–CNRS) for computing facilities. N.O. is grateful to the French Ministry of Foreign Affairs for a travel grant (CMEP 02 MDU 552).

Appendix

Extended Hückel calculations [45] were carried out on model compounds derived from the experimental structures using the CACAO programme [46]. Standard Slater exponents and valence-shell ionisation potentials were used [46]. DFT calculations were carried out on model compounds using the Amsterdam Density Functional (ADF) program [47] developed by Baerends and coworkers [48]. Electron correlation was treated within the local density approximation (LDA)

in the Vosko–Wilk–Nusair parameterisation [49]. The non-local corrections of Becke and Perdew were added to the exchange and correlation energies, respectively [50,51]. The atom electronic configurations were described by a triple- ζ Slater-type orbital (STO) basis set for H 1s, C 2s and 2p, O 2s and 2p, P 3s and 3p, and I 5s and 5p, augmented with a 3d single- ζ polarisation function for C, O, P atoms, with a 5d single- ζ polarisation function for I atom, and with a 2p single- ζ polarisation function for H atoms. The atom electronic configurations of the metal atoms were also described by a triple- ζ STO for the outer n d and $(n + 1)$ s orbitals augmented with a single- ζ STO for the outer $(n + 1)$ p orbitals (ADF basis set TZP) and with a frozen core approximation for the shells of lower energy. Geometry optimisations were carried out using the analytical gradient method implemented by Verluise and Ziegler [52]. For the tungsten and platinum molecules, relativistic corrections were added using the zeroth order regular approximation (ZORA) scalar Hamiltonian [53]. Representations of the molecular orbitals were done using MOLEKEL4.1 [54].

References

- [1] R. Hoffmann, *The Same and Not the Same*, Columbia University Press, New York, 1995 (p. 231).
- [2] For theoretical studies, see for example: (a) J.K. Burdett, T.J. McLarnan, *Inorg. Chem.* 21 (1982) 1119; (b) G.J. Miller, J.K. Burdett, C. Schwarz, A. Simon, *Inorg. Chem.* 25 (1986) 4437.
- [3] A. Simon, *Angew. Chem. Int. Ed. Engl.* 27 (1988) 159.
- [4] (a) E. Warkentin, R. Masse, A. Simon, *Z. Anorg. Allg. Chem.* 491 (1982) 323. For a theoretical study see: (b) S. Satpathy, O. Andersen, *Inorg. Chem.* 24 (1985) 2604.
- [5] See for example: (a) M. Akita, Y. Moro-oka, *Bull. Chem. Soc. Jpn.* 68 (1995) 420; (b) U. Rosenthal, *Angew. Chem. Int. Ed. Engl.* 42 (2003) 1794; (c) M.I. Bruce, P.J. Low, *Adv. Organomet. Chem.* 50 (2004) 179; (d) J.P. Selegue, *Coord. Chem. Rev.* 248 (2004) 1543.
- [6] M. St. Clair, W.P. Schaefer, J.E. Bercaw, *Organometallics* 10 (1991) 525.
- [7] (a) M.I. Bruce, M.R. Snow, E.R. Tiekink, M.L. Williams, *J. Chem. Soc. Chem. Commun.* (1987) 701; (b) C.J. Adams, M.I. Bruce, B.W. Skelton, A.H. White, *J. Chem. Soc. Chem. Commun.* (1992) 26.
- [8] A. Arrigoni, A. Ceriotti, R. Della Pergola, M. Manassero, N. Maschiocchi, M. Sansoni, *Angew. Chem. Int. Ed. Engl.* 23 (1984) 322.
- [9] G.A. Koutsantonis, J.-P. Selegue, *J. Am. Chem. Soc.* 113 (1991) 2316.
- [10] (a) R.E. Lapointe, P.T. Wolczanski, J.F. Mitchell, *J. Am. Chem. Soc.* 108 (1986) 6382; (b) D.R. Neithamer, R.E. Lapointe, R.A. Wheeler, D.S. Richeson, G.D. Duyne, P.T. Wolczanski, *J. Am. Chem. Soc.* 111 (1989) 9056.
- [11] (a) T.M. Gilbert, R.D. Rogers, *J. Organomet. Chem.* 421 (1991) C1; (b) K.G. Caulton, R.H. Cayton, M.H. Chisholm, J.C. Huffman, E.B. Lobkovsky, Z. Xue, *Organometallics* 11 (1992) 321.
- [12] (a) J.-F. Halet, D.M.P. Mingos, *Organometallics* 7 (1988) 51; (b) J.-F. Halet, in: M. Gielen (Ed.), *Topics in Physical Organometallic Chemistry*, vol. 4, Freund Publishing House, London, 1992, p. 221.
- [13] (a) G. Frapper, J.-F. Halet, *Organometallics* 14 (1995) 5044; (b) G. Frapper, J.-F. Halet, M.I. Bruce, *Organometallics* 16 (1997) 2590; (c) C.J. Adams, M.I. Bruce, B.W. Skelton, A.H. White, G. Frapper, J.-F. Halet, *J. Chem. Soc. Dalton Trans.* (1997) 371; (d) C.J. Adams, M.I. Bruce, J.-F. Halet, S. Kahlal, B.W. Skelton, A.H. White, *J. Chem. Soc. Dalton Trans.* (2001) 414.
- [14] C. Zheng, Y. Apeloig, R. Hoffmann, *J. Am. Chem. Soc.* 110 (1998) 749.
- [15] J. Heidrich, M. Steimann, M. Appel, W. Beck, J.R. Phillips, W.C. Troger, *Organometallics* 9 (1990) 1296.
- [16] P. Belanzoni, N. Re, A. Sgamellotti, C. Floriani, *J. Chem. Soc., Dalton Trans.* (1997) 4773.
- [17] P. Belanzoni, N. Re, M. Rosi, A. Sgamellotti, C. Floriani, *Organometallics* 15 (1996) 4264.
- [18] W.J. Evans, G.W. Rabe, J.W. Ziller, *J. Organomet. Chem.* 483 (1994) 21.
- [19] P. Binger, P. Müller, P. Phillips, B. Gabor, R. Mynott, A.T. Herrmann, F. Langhauser, C. Krüger, *Chem. Ber.* 125 (1992) 2209.
- [20] D. Thomas, N. Peulecke, V.V. Burlakov, B. Heller, W. Baumann, A. Spannenberg, R. Kempe, U. Rosenthal, R.Z. Beckhaus, *Allg. Chem.* 624 (1998) 919.
- [21] C.J. Harlan, J.A. Tunge, B.M. Bridgewater, J.R. Norton, *Organometallics* 19 (2000) 2365.
- [22] G.E. Southard, M.D. Curtis, J.W. Kampf, *Organometallics* 15 (1996) 4667.
- [23] M.-C. Chen, Y.-J. Tsai, C.-T. Chen, Y.-C. Lin, T.-W. Tseng, G.-H. Lee, Y. Wang, *Organometallics* 10 (1991) 378.
- [24] Y.-L. Yang, L.J.-J. Wang, Y.-C. Lin, S.-L. Huang, M.-C. Chen, G.-H. Lee, Y. Wang, *Organometallics* 16 (1997) 1573.
- [25] J.A. Davies, M. El-Ghanam, A.A. Pinkerton, D.A. Smith, *J. Organomet. Chem.* 409 (1991) 367.
- [26] J. Heidrich, M. Steimann, M. Appel, W. Beck, J.R. Phillips, W.C. Troger, *Organometallics* 9 (1990) 1296.
- [27] M. Akita, M.-C. Chung, A. Sakurai, S. Sugimoto, M. Terada, M. Tanaka, Y. Moro-Oka, *Organometallics* 16 (1997) 4882.
- [28] M.I. Bruce, K. Costuas, B.G. Ellis, J.-F. Halet, N. Ouddai, G.S. Perkins, B.W. Skelton, A.H. White, Unpublished results.
- [29] H. Ogawa, K. Onitsuka, T. Joh, S. Takahashi, Y. Yamamoto, H. Yamasaki, *Organometallics* 7 (1988) 2257.
- [30] K. Sunkel, U. Birk, C. Robl, *Organometallics* 13 (1994) 1679.
- [31] J.R. Berenguer, J. Fornies, E. Lalinde, F. Martinez, *Organometallics* 14 (1995) 2532.
- [32] V.W.-W. Yam, K.M.-C. Wong, N. Zhu, *Angew. Chem. Int. Ed. Engl.* 42 (2003) 1400.

- [33] R.-Y. Liao, A. Schier, H. Schmidbaur, *Organometallics* 22 (2003) 3199.
- [34] M.I. Bruce, K.R. Grundy, M.J. Liddell, M.R. Snow, E.R. Tiekink, *J. Organomet. Chem.* 344 (1988) C49.
- [35] C.-M. Che, H.-Y. Chao, V.M. Miskowski, Y. Li, K.-K. Cheung, *J. Am. Chem. Soc.* 123 (2001) 4985.
- [36] T.E. Müller, D.M.P. Mingos, D.J. Williams, *J. Chem. Soc. Chem. Commun.* (1994) 1787.
- [37] T.E. Müller, S.W.K. Choi, D.M.P. Mingos, D. Murphy, D.J. Williams, V.W.-W. Yam, *J. Organomet. Chem.* 484 (1994) 209.
- [38] F.R. Lemke, D.J. Szalda, R.M. Bullock, *J. Am. Chem. Soc.* 113 (1991) 8466.
- [39] (a) J.A. Ramsden, W. Weng, A.M. Arif, J.A. Gladysz, *J. Am. Chem. Soc.* 114 (1992) 5890; (b) W. Weng, T. Bartik, M. Brady, B. Bartik, J.A. Ramsden, A.M. Arif, J.A. Gladysz, *J. Am. Chem. Soc.* 117 (1995) 11922.
- [40] J. Lauher, R. Hoffmann, *J. Am. Chem. Soc.* 98 (1976) 1729.
- [41] P. Kubacek, R. Hoffmann, Z. Havlas, *Organometallics* 1 (1982) 180.
- [42] B.E.R. Schilling, R. Hoffmann, D.L. Lichtenberger, *J. Am. Chem. Soc.* 101 (1979) 585.
- [43] T.A. Albright, J.K. Burdett, M.-H. Whangbo, *Orbital Interactions in Chemistry*, Wiley, New York, 1985.
- [44] R. Hoffmann, *Angew. Chem. Int. Ed. Engl.* 21 (1982) 711.
- [45] R. Hoffmann, *J. Chem. Phys.* 39 (1963) 1397.
- [46] C. Mealli, D. Proserpio, *J. Chem. Ed.* 67 (1990) 399.
- [47] Amsterdam Density Functional (ADF) Program, release 2002.01, SCM, Vrije Universiteit, Amsterdam, The Netherlands (<http://www.scm.com>).
- [48] (a) E.J. Baerends, D.E. Ellis, P. Ros, *Chem. Phys.* 2 (1973) 41; (b) G. te Velde, E.J. Baerends, *J. Comput. Phys.* 99 (1992) 84; (c) C. Fonseca Guerra, J.G. Snijders, G. te Velde, E.J. Baerends, *Theo. Chim. Acc.* 99 (1998) 391; (d) F.M. Bickelhaupt, E.J. Baerends, *Rev. Comput. Chem.* 15 (2000) 1; (e) G. te Velde, F.M. Bickelhaupt, C. Fonseca Guerra, S.J.A. van Gisbergen, E.J. Baerends, J.G. Snijders, T. Ziegler, *J. Comput. Chem.* 22 (2001) 931.
- [49] S.D. Vosko, L. Wilk, M. Nusair, *Can. J. Chem.* 58 (1990) 1200.
- [50] (a) A.D. Becke, *J. Chem. Phys.* 84 (1986) 4524; (b) A.D. Becke, *A.D. Phys. Rev. A* 38 (1988) 3098.
- [51] (a) J.P. Perdew, *Phys. Rev. B* 33 (1986) 8822; (b) J.P. Perdew, *Phys. Rev. B* 34 (1986) 7406.
- [52] L. Verluise, T. Ziegler, *J. Chem. Phys.* 88 (1988) 322.
- [53] (a) E. van Lethe, E.J. Baerends, J.G. Snijders, *J. Chem. Phys.* 99 (1993) 4597; (b) E. van Lethe, E.J. Baerends, J.G. Snijders, *J. Chem. Phys.* 101 (1994) 9783; (c) E. van Lethe, R. van Leeuwen, E.J. Baerends, J.G. Snijders, *Int. J. Quantum Chem.* 57 (1996) 281.
- [54] P. Flükiger, H.P. Lüthi, S. Portmann, J. Weber, Swiss Center for Scientific Computing (CSCS), Switzerland, 2000–2001.